International Journal of Nanomedicine

Dovepress
Taylor & Francis Group

Open Access Full Text Article

ORIGINAL RESEARCH

Development of a Rifapentine-Loaded Alendronate-Conjugated PLGA-PEG Nanosystem: A Novel Bone-Targeted Strategy for Osteoarticular Tuberculosis Treatment with Enhanced Drug Delivery and Bone Regeneration

Zhen Wang[1–3,*], Hong Wei[4,*], Xiaopeng Qiu[4], Bo Zhao[4], Ziquan Yang[5]

[1]Department of Orthopedics, South China Hospital, Medical School, Shenzhen University, Shenzhen, Guangdong, 518116, People's Republic of China; [2]Guangdong Key Laboratory for Biomedical Measurements and Ultrasound Imaging, National-Regional Key Technology Engineering Laboratory for Medical Ultrasound, School of Biomedical Engineering, Shenzhen University Medical School, Shenzhen, Guangdong, 518060, People's Republic of China; [3]Department of Orthopedics, Linfen Hospital of Shanxi Medical University, Linfen, Shanxi, 041000, People's Republic of China; [4]Department of Health Examination Center, Linfen Hospital of Shanxi Medical University, Linfen, Shanxi, 041000, People's Republic of China; [5]Department of Orthopedics, First Hospital of Shanxi Medical University, Taiyuan, Shanxi, 030000, People's Republic of China

*These authors contributed equally to this work

Correspondence: Zhen Wang, Department of Orthopedics, South China Hospital, Medical School, Shenzhen University, Shenzhen, Guangdong, 518116, People's Republic of China, Email 421252955@qq.com; Ziquan Yang, Department of Orthopedics, First Hospital of Shanxi Medical University, Taiyuan, Shanxi, 030000, People's Republic of China, Email yzqsdyy@126.com

International Journal of Nanomedicine downloaded from https://www.dovepress.com/
For personal use only.

Background: The treatment of osteoarticular tuberculosis (TB) remains a significant clinical challenge, primarily due to inadequate drug delivery to bone tissues, severe bone destruction, and delayed repair processes. Conventional pharmacological therapy has limited efficacy and often necessitates surgical intervention. Thus, we developed a bone-targeted nanosystem by integrating rifapentine (RPT) and alendronate (ALN) to improve drug delivery, mitigate TB-induced bone destruction, and facilitate bone regeneration.

Methods: In this study, ALN was conjugated to PLGA-PEG-COOH utilizing the DCC/NHS method and subsequently loaded with RPT through premix membrane emulsification, resulting in the formation of the RPT/ALN-PLGA-PEG nanosystems. The physicochemical properties of the nanosystems were characterized, and its antibacterial activity, cytotoxicity, and impact on osteogenic/osteoclastic differentiation were evaluated in vitro. Bone-targeting efficacy and biodistribution were assessed using in vivo experiments. A rabbit spinal TB model was used to assess therapeutic efficacy based on inflammatory and bone turnover markers, bone mineral density (BMD), and histopathological analyses.

Results: The RPT/ALN-PLGA-PEG nanosystems exhibited a uniform size of 89 nm, excellent stability, and sustained drug-release characteristics. In vitro, the nanosystems demonstrated excellent antibacterial activity, low cytotoxicity, and the ability to suppress osteoclastogenesis while promoting osteoblast differentiation. In vivo imaging and tissue distribution studies have demonstrated that the RPT/ALN-PLGA-PEG nanosystem achieved a drug concentration in bone tissue at least 3-fold higher than that of the non-targeted nanosystem. In vivo, the bone-targeted nanosystem effectively alleviated inflammation, stabilized levels of bone resorption markers, and improved BMD, accompanied by elevated levels of osteogenic markers. Histological scores revealed complete bone regeneration in the RPT/ALN-PLGA-PEG group, whereas fibrous tissue formation was observed in the other groups.

Conclusion: The RPT/ALN-PLGA-PEG nanosystems demonstrated remarkable bone-targeting capability, sustained and potent antibacterial efficacy, and mitigation of bone destruction, coupled with the promotion of bone repair. These findings provide an innovative approach for addressing osteoarticular TB.

Keywords: bone targeting, bone regeneration, nanosystems, osteoarticular tuberculosis, alendronate

Received: 30 July 2025
Accepted: 20 November 2025
Published: 2 December 2025

© 2025 Wang et al. This work is published and licensed by Dove Medical Press Limited. The full terms of this license are available at https://www.dovepress.com/terms.php and incorporate the Creative Commons Attribution – Non Commercial (unported, v4.0) License (http://creativecommons.org/licenses/by-nc/4.0/). By accessing the work you hereby accept the Terms. Non-commercial uses of the work are permitted without any further permission from Dove Medical Press Limited, provided the work is properly attributed. For permission for commercial use of this work, please see paragraphs 4.2 and 5 of our Terms (https://www.dovepress.com/terms.php).

Introduction

Tuberculosis (TB), caused by *Mycobacterium tuberculosis*, is a chronic and debilitating infectious disease that remains a significant public health challenge globally. Osteoarticular TB is a common form of extrapulmonary TB. Compared to TB at other anatomical sites, osseous tissue exhibits greater rigidity and less blood supply. This increases vulnerability to necrosis, encapsulation, and calcification, which impair drug delivery efficiency and targeting accuracy, thereby extending treatment duration, reducing therapeutic efficacy, and affecting patient compliance in osteoarticular TB.[1,2] Additionally, TB-induced local bone necrosis often leads to the development of bone defects, which frequently require surgical intervention.[3] Therefore, improving drug delivery and mitigating bone destruction while promoting bone defect repair is more critical for treating osteoarticular TB than drug molecule innovation.

Nanosystems have become a promising method for drug delivery, improving drug stability, extending release duration,[4] and reducing side effects, while maintaining or improving therapeutic efficacy.[5] Polylactide-co-glycolide (PLGA) nanoparticles have received approval from the United States Food and Drug Administration and the European Medicines Agency[6] as delivery carrier materials for controlled drug delivery. This is due to their excellent biocompatibility, safety, and biodegradability, with degradation byproducts being naturally eliminated via metabolic pathways.[7] Most nanosystems are synthesized with polyethylene glycol (PEG), which is conjugated to enhance the stability and efficiency of the system, thereby extending its circulation time in the bloodstream.[8]

Compared to rifampicin, a widely used first-line anti-TB drug, rifapentine (RPT) exhibits a comparable antibacterial spectrum, while demonstrating 2–10 times greater anti-TB efficacy. Additionally, RPT is associated with a lower incidence of adverse reactions and a longer half-life.[9] Furthermore, compared to other water-soluble anti-TB medications, RPT exhibits superior stability and minimized leakage both in vitro and in vivo following the development of targeted formulations.

Histopathological analysis revealed that the activation of osteoclasts in specific areas is crucial for the bone destruction associated with osteoarticular TB.[10] Consequently, the increased number and improved activation of osteoclasts following *Mycobacterium tuberculosis* infection serve as key contributors to its pathogenesis.[11] Bisphosphonates, acidic oligopeptides, and tetracycline are commonly utilized as targeting strategies for the delivery of drugs to bone surfaces.[12] Alendronate (ALN), in the form of ALN acid, is a nitrogen-containing bisphosphonate. These bisphosphonates can bind hydroxyapatite in the bone matrix[13] and inhibit osteoclast activity during bone resorption. Given that ALN can directly regulate bone metabolism and inhibit osteoclast activity, while demonstrating significant bone-targeting efficacy,[14] we hypothesize that the combination of RPT and ALN may synergistically affect the treatment of osteoarticular TB.

In this study, an ALN-functionalized drug delivery nanosystem was developed to prolong the circulation duration of drugs and achieve efficient, targeted delivery to the bone tissue. This bone-targeted nanosystem aims to improve RPT accumulation in bone tissue, prolong drug release, improve anti-TB efficacy, inhibit osteoclast activity to mitigate bone destruction caused by *Mycobacterium tuberculosis*, and promote bone regeneration during treatment (Figure 1).

Materials and Methods

Animals and Reagents

The animals used in this study were obtained from the Experimental Animal Research Center of Shanxi Medical University. Approval for this study was granted by the Animal Ethics Committee of the Affiliated Linfen Hospital of Shanxi Medical University (Approval Number: IACUC-20220829005). All animal care and experimental procedures were conducted in accordance with the guidance of the Care and Use of Laboratory Animals from the National Institutes of Health.

Unless otherwise specified, all chemicals and reagents were acquired from Solarbio Science & Technology Co., Ltd. (Beijing, China). ALN (Sigma-Aldrich, St Louis, Missouri, USA), RPT (Solarbio Science & Technology Co., Ltd), PLGA-PEG-COOH (Mw: 12,000, lactide: glycolide = 50:50, Jinan Daigang Biomaterial Co., Ltd, Shandong, China), Dicyclohexylcarbodiimide (DCC) and N-hydroxysuccinimide (NHS) were obtained from Sigma-Aldrich. Cell Counting Kit-8 (Dojindo, Kumamoto, Japan), Shirasu porous glass (SPG) membranes (SPG Technology Co., Ltd, Miyazaki,

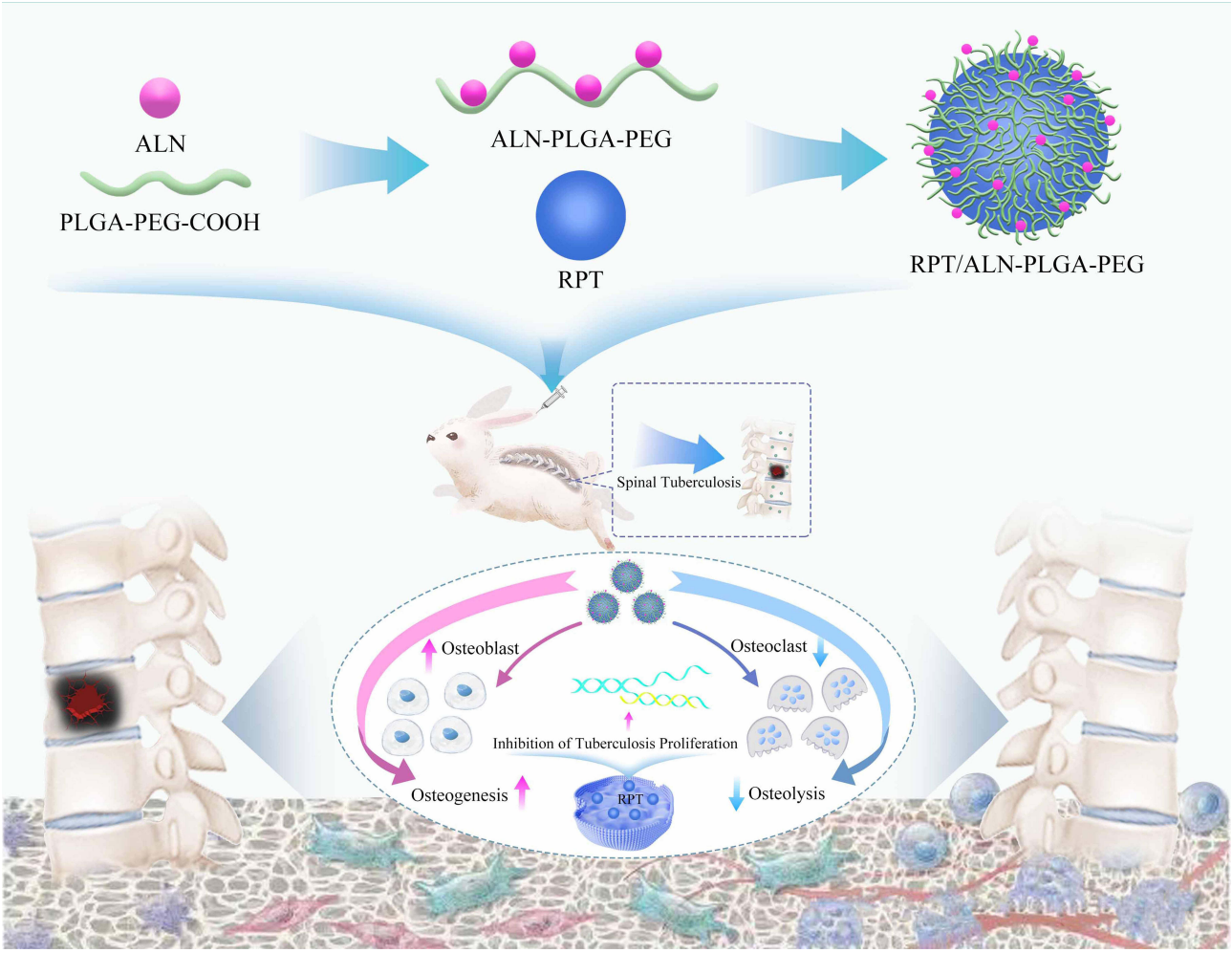

Figure 1 Synthesis and mechanism of RPT/ALN-PLGA-PEG nanosystems for targeted therapy of osteoarticular Tuberculosis.

Japan), Alpha Modified Eagle's Minimum Essential Medium (α-MEM), Dulbecco's modified Eagle's medium (DMEM), trypsin, fetal bovine serum (FBS) and penicillin-streptomycin solution were acquired from Thermo Fisher Scientific (Waltham, MA, USA). The Xinjiang Academy of Animal Science supplied the *Mycobacterium tuberculosis* strains.

Synthesis of ALN-PLGA-PEG Conjugates

The ALN-PLGA-PEG conjugates were synthesized using the DCC/NHS method (Figure 2A). Approximately 26 mg of ALN was dissolved in 5 mL of 5% acetic acid solution and freeze-dried to obtain acidified ALN for later use. A solution containing 240 mg of PLGA-PEG-COOH, 8.24 mg of DCC, and 2.3 mg of NHS was prepared in 20 mL of anhydrous dimethyl sulfoxide (DMSO) and stirred for 24 h under nitrogen protection to activate the carboxylic acid group. The resulting precipitate was removed via filtration. The acidified ALN was then added to the activated PLGA-PEG solution and stirred under nitrogen protection for 24 h. Using a membrane with a molecular weight cut-off (MWCO) of 3.5 kDa, the mixture was dialyzed in deionized water for a period of 48 h. The mixture was centrifuged at 15,000 × g for 15 min, washed thrice with deionized water, lyophilized, and stored for subsequent experiments.

Development of Bone-Targeted Drug Delivery Nanosystems

Bone-targeted nanosystems (RPT/ALN-PLGA-PEG) were synthesized using the premix membrane emulsification method. RPT (5 mg) and ALN-PLGA-PEG (60 mg) were dissolved in 5 mL dichloromethane (DCM) and cooled to 4 °C. A primary emulsion was formed by subjecting the solution to probe sonication with a sonicator (UP400S, Hielscher

https://doi.org/10.2147/IJN.S478893

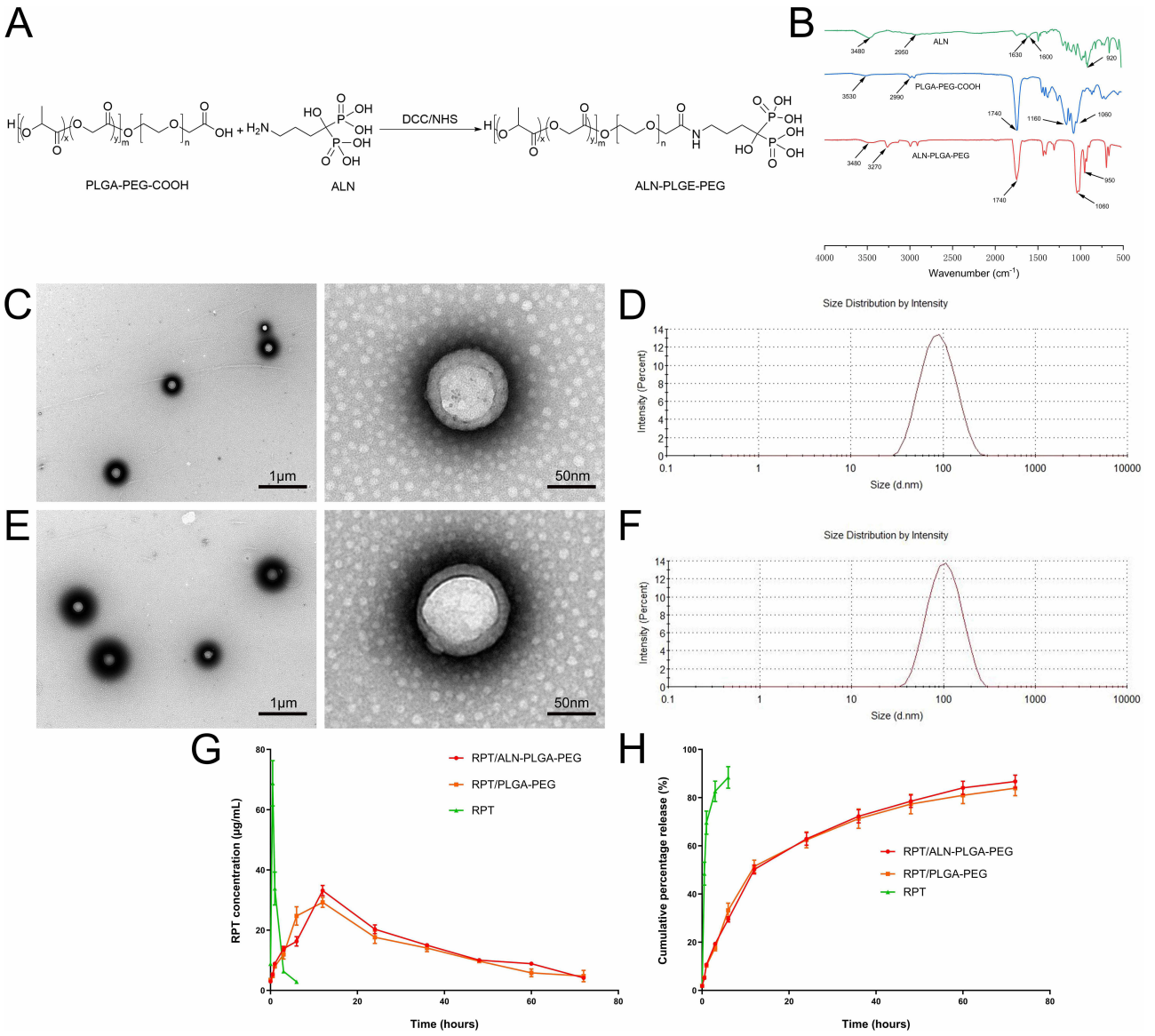

Figure 2 Characterization of nanosystems. Illustrative chemical synthesis of ALN-PLGA-PEG (**A**). FTIR spectra of ALN, PLGA-PEG-COOH, and ALN-PLGA-PEG (**B**). Transmission electron microscopy images and particle size distributions of RPT/PLGA-PEG (**C** and **D**) and RPT/ALN-PLGA-PEG nanosystems (**E** and **F**), respectively (scale bar = 1μm, scale bar = 50 nm). In vitro RPT release curves (**G**) and cumulative percentage release curve (**H**) of free RPT, RPT/PLGA-PEG, and RPT/ALN-PLGA-PEG.

Ultrasonics, Germany) at 50% amplitude for 1.5 min. To generate a coarse emulsion, the emulsion was subjected to further emulsification using a 1 μm pore-sized SPG membrane while being magnetically stirred for 5 min. Subsequently, a SPG membrane with a pore size of 0.1 μm was utilized to subject the coarse emulsion to five cycles of high-pressure homogenization. The resulting emulsion was immediately transferred into 50 mL of 1% (w/v) PVA solution and stirred magnetically at 5 × g overnight to facilitate evaporation of the organic solvent. The separated nanoparticles were collected by centrifugation, washed three times with deionized water, and lyophilized. Non-targeted nanosystems (RPT/PLGA-PEG) were developed using an identical procedure. The only modification to the procedure for the preparation of fluorescently labeled nanosystems was the addition of Cy5.5 to DCM.

Characterization of Nanosystems

The synthesized ALN, PLGA-PEG-COOH, and ALN-PLGA-PEG were analyzed by Fourier Transform Infrared (FTIR) spectrometer (Nicolet 8700, Thermo Fisher Scientific). The spectra were captured at 500–4000 cm^{-1}. These conjugates

were confirmed further through ^{1}H NMR spectroscopy on a Bruker spectrometer (Bruker, Switzerland). The particle size, zeta potential (ZP), and polydispersity index (PDI) of the RPT/ALN-PLGA-PEG and RPT/PLGA-PEG nanosystems were determined using the ZetaSizer Nano-ZS (Malvern Instruments Ltd., Malvern, UK). 5 mg of nanoparticles were weighed into a 10 mL flask, and 0.1 mL of DCM was added to disrupt their structure. The drug loading efficiency (DLE) and encapsulation efficiency (EE) were assayed by ultraviolet spectrophotometry. The morphology of the nanosystems were examined using a JEM-1230 transmission electron microscope (TEM; JEOL, Tokyo, Japan) following staining with a 2% (w/v) sodium phosphotungstate solution. The stability was assessed by storing the samples at 25 °C for 20 days in a controlled chamber, with periodic measurements of particle size and ZP.

Drug Release Properties in vitro

The study on drug release was conducted using the dialysis method. Free RPT, RPT/PLGA-PEG, and RPT/ALN-PLGA-PEG nanosystems were enclosed in a dialysis bag (MWCO 3.0 kDa) and incubated in phosphate-buffered saline (PBS) at 37 °C with stirring at 100 rpm. Samples were collected at specific intervals, replaced with equal volume liquid, and analyzed using ultraviolet spectrophotometry method. RPT concentration was determined by comparing it with the standard curve. The procedure was performed three times, and the curves for drug release and cumulative drug release percentages were plotted.

In vitro Antibacterial Activity

The antibacterial efficacy of RPT/ALN-PLGA-PEG against *Mycobacterium tuberculosis* H37Rv (ATCC 27294) was assessed using the agar disk diffusion method. *Mycobacterium tuberculosis* suspension (approximately 1×10^{6} cfu/mL) was prepared, and 20 mg of RPT/ALN-PLGA-PEG were suspended in 10 mL of PBS for 6 h. A sterile filter paper (6 mm in diameter) was soaked in the suspension for 30 min. Approximately 100 μL of the bacterial suspension was spread onto a modified Lowenstein-Jensen medium, with filter paper positioned at the center. The medium was then incubated at 37 °C in an atmosphere containing 5% CO_2 for 3–4 weeks to observe the inhibition zone. RPT and RPT/PLGA-PEG nanosystems were used as positive controls, while filter paper without the drug served as the negative control.

In vitro Cytotoxicity Assessment

Bone marrow mesenchymal stem cells (BMSCs) were isolated from the tibias and femurs of 6-week-old C57BL/6J mice and cultured using a previously described method.[15] The cytotoxicity of nanosystems was evaluated using the Cell Counting Kit-8 (CCK-8) assay. BMSCs were divided into five groups and cultured in a 96-well plate at a density of 5×10^{3} cells/mL, with each group in three wells. The cells were treated with ALN, ALN-PLGA-PEG, and RPT/ALN-PLGA-PEG nanosystems at final concentrations equivalent to ALN (0, 0.03, 0.3, 3, and 10.0 μg/mL)[16] at 37 °C for 48 h. The ALN content in the formulation was quantified using spectrophotometry based on complex formation with Fe (III) ions.[17] RPT, RPT/PLGA-PEG, and RPT/ALN-PLGA-PEG nanosystems were incubated with BMSCs at final RPT-equivalent concentrations (0, 15.0, 30.0, 45.0, and 60.0 μg/mL)[18,19] for 48 h, following the same procedure. Absorbance at 450 nm was recorded with a Multiskan MK3 microplate spectrophotomete (Thermo Fisher Scientific).

Cellular Uptake Experiments

Bone marrow monocytes (BMMs) were isolated from the femurs of 4–6-week-old C57BL/6J mice and cultured for 4 days in α-MEM supplemented with 10% FBS, 1% penicillin-streptomycin, and 30 ng/mL macrophage colony-stimulating factor (M-CSF, R&D Systems, Minneapolis, MN, USA, catalog no. 416-ML). The adherent cells were collected as BMMs. For the cellular uptake assay, BMMs were cultured in 24-well plates at a density of 1×10^{4} cells/well. After a 24-hour incubation period, the medium was exchanged for fresh medium containing Cy5.5-labeled RPT/PLGA-PEG or RPT/ALN-PLGA-PEG nanosystems (50 μg/mL). Non-internalized nanoparticles were removed by washing the wells with cold PBS at 2 and 6 h. Cells were fixed with 4% paraformaldehyde for 15 min, subsequently stained with phalloidin for 15 min to label the cytoskeleton, and counterstained with DAPI for 5 min to visualize the nuclei. The samples were then analyzed using an Olympus FV3000 confocal laser scanning microscope (CLSM; Tokyo, Japan).

In vivo Assessment of Biodistribution, Biosafety, and Targeting Efficiency

C57BL/6J mice were used to investigate the in vivo biodistribution of nanosystems. The mice were divided into three groups based on the administration of different formulations via tail vein injection: RPT/ALN-PLGA-PEG, RPT/PLGA-PEG, and free RPT. An equivalent dose of RPT (10 mg/kg) was administered to all groups. Tissue samples were collected from 20% (w/v) tissue homogenates at 1, 24, and 48 h post-injection for drug concentration analysis. High-performance liquid chromatography was used to evaluate the distribution of RPT and quantify its concentration in plasma, liver, kidney, and bone tissues.

The potential hepatotoxicity and nephrotoxicity associated with the nanosystem were assessed by measuring key serum biomarkers in each group on the fourth day post-injection, with saline administration serving as the control. The biomarkers included alanine transaminase (ALT), aspartate transaminase (AST), creatinine (Cr), and blood urea nitrogen (BUN). These biomarkers were analyzed using a Hitachi 7100 automatic biochemical analyzer (Tokyo, Japan).

To evaluate the bone-targeting efficacy, Cy5.5-labeled RPT/ALN-PLGA-PEG nanosystems (10 mg/kg) were administered intravenously post-anesthesia, with the control group receiving non-targeted RPT/PLGA-PEG nanosystems. In vivo real-time fluorescence was monitored using the in vivo imaging system (IVIS) Spectrum CT Imaging System (PerkinElmer, Waltham, MA, USA). Additionally, 24 h after the injection, fluorescence analysis of the brain, lungs, heart, liver, spleen, kidneys, and bones was performed using the same system.

Impact of Nanosystems on Osteogenic and Osteoclastic Differentiation

BMSCs and BMMs were cultured in 96-well plates at a density of 1×10^3 cells/well. BMSCs were maintained in osteogenic induction medium to promote their differentiation into osteoblasts. BMMs were cultured in α-MEM supplemented with 30 ng/mL M-CSF and 50 ng/mL receptor activator of nuclear factor-κB ligand (RANKL, R&D Systems, catalog no. 462-TEC) to induce their differentiation into osteoclasts. BMSCs and BMMs were respectively divided into four groups based on the administration of ALN-loaded formulations: the RPT/ALN-PLGA-PEG group, the ALN-PLGA-PEG group, the ALN group, and the Control group. The final concentration in each experimental group was standardized to the equivalent of ALN (3 μg/mL), whereas the Control group received the cell culture medium only. Following a 7-day culture period, commercially available staining kits were employed to perform alkaline phosphatase (ALP) and Alizarin red staining on BMSCs, whereas Tartrate-resistant acid phosphatase (TRAP) staining was conducted on BMMs. All procedures were performed according to the manufacturer's protocols.

Western Blot Analysis

Total protein was extracted from BMSCs and BMMs, and the protein concentrations were determined using the bicinchoninic acid (BCA) assay kit. Equal amounts of protein samples were separated using sodium dodecyl sulfate-polyacrylamide gel electrophoresis and transferred onto polyvinylidene fluoride membranes (Merck Millipore, Mannheim, Germany). The membranes were incubated overnight at 4 °C with primary antibodies against Collagen I (Abcam, Cambridge, UK, rabbit monoclonal, catalog no. ab270993, dilution 1:1000), osteocalcin (Abcam, rabbit monoclonal, catalog no. ab309521, dilution 1:1000) for BMSCs, nuclear factor of activated T-cells cytoplasmic 1 (NFATc1, Abcam, rabbit polyclonal, catalog no. ab25916, dilution 1:1000), cellular oncogene fos (c-Fos, Abcam, rabbit monoclonal, catalog no. ab222699, dilution 1:1000) for BMMs, and GAPDH (Abcam, rabbit monoclonal, catalog no. ab181602, dilution 1:10000) as an internal control. The membranes were then incubated with horseradish peroxidase-conjugated goat anti-rabbit IgG (Abcam, catalog no. ab97051, dilution 1:5000) for 1.5 h at room temperature. Protein bands were detected using an enhanced chemiluminescence (ECL) detection kit (Thermo Fisher Scientific) and visualized with a chemiluminescence imaging system (Bio-Rad, Hercules, CA, USA). Subsequently, the optical density was quantified using the ImageJ software (NIH, Bethesda, Maryland).

Development of Osteoarticular Tuberculosis Models

The animal model of spinal TB was established according to the previously described method.[15] Forty-eight male New Zealand white rabbits were anesthetized, and the fifth lumbar vertebra was surgically exposed. A steel drill bit was utilized to create a standardized bone defect (1.5 mm in diameter and depth) at the proximal root of the transverse process

of the fifth lumbar vertebra. Subsequently, 0.1 mL of *Mycobacterium tuberculosis* suspension (H37Rv ATCC 27294, 1×10^6 cfu/mL) was gradually infused into the defect. One week later, the animals were randomly divided into four groups based on the administration of RPT-loaded formulations: the RPT/ALN-PLGA-PEG group, the RPT/PLGA-PEG group, the RPT group, and a Control group that received physiological saline. The final RPT-equivalent concentrations in the treatment groups were standardized to 30 mg/kg body weight and administered intravenously twice a week for 4 or 8 weeks.

Impact of Nanosystems on Inflammation and Bone Turnover Markers

Blood samples were collected from the four groups at different stages: before TB infection (normal), 1 week post-infection (TB); and 1, 2, 4, and 8 weeks post-treatment. The erythrocyte sedimentation rate (ESR) was measured using an Electa-Lab ESR analyzer (Forli, Italy). The concentrations of C-reactive protein (CRP) in serum were measured using a CRP enzyme-linked immunosorbent assay (ELISA) kit (Abcam, catalog no. Ab157726), following the manufacturer's instructions. Serum concentrations of bone alkaline phosphatase (BALP) and N-terminal propeptide of type 1 procollagen (P1NP), which serve as indicators of bone formation, were measured using ELISA kits supplied by CUSABIO Biotech Co., Ltd (Wuhan, China; BALP: catalog no. CSB-E15042Rb; P1NP: catalog no. CSB-E17085Rb). Furthermore, serum levels of two key bone resorption markers, C-terminal telopeptides of collagen type I (CTX-I) and tartrate-resistant acid phosphatase 5b (TRAP-5b), were quantified using ELISA kits provided by Fine Biotech Co., Ltd (Wuhan, China; CTX-I: catalog no. ERB0038) and CUSABIO (TRAP-5b: catalog no. CSB-E15043Rb), respectively. The absorbance at 450 nm was recorded with a Multiskan Spectrum microplate reader manufactured by Thermo Fisher Scientific.

Evaluation of Bone Mineral Density (BMD)

Following the administration of anesthesia, the rabbit spine was scanned at a standard position using a dual-energy X-ray absorptiometry (DXA) scanner (OsteoSys, Seoul, Korea). The lateral surface of the vertebra was aligned to face the scanner plate. Scans were performed at the same stages as in the prior experiment to assess the BMD of the affected spinal areas.

Histological Examination and Scoring

The rabbits were euthanized using sodium pentobarbital 4 and 8 weeks post-treatment to collect the diseased tissue. After macroscopic examination, the samples were fixed using formalin, decalcified, paraffin-embedded, and sectioned into 5 mm slices. Hematoxylin and eosin (HE) staining was conducted on sections from embedded samples for evaluating tissue morphology. Three observers independently evaluated the regenerated tissue in the areas of bone destruction using Nilsson histological scores (NHS).[20]

Statistical Analysis

The data were analyzed using the SPSS software (version 22.0; IBM, Armonk, NY, USA). The results are presented as mean ± standard deviation. Differences between continuous variables were assessed using one-way analysis of variance with post-hoc multiple comparisons (Tukey's and Games-Howell tests). A $p < 0.05$ indicated statistical significance.

Results

Physical and Chemical Characterization

The infrared spectra of ALN, PLGA-PEG-COOH, and ALN-PLGA-PEG are depicted in Figure 2B. The ALN spectrum exhibited bands at 3480 (O-H of phosphate), 2950 (C-H), 1630 (N-H), and 920 (P-O) cm^{-1}.[21] In the PLGA-PEG-COOH spectrum, the band at 2990 cm^{-1} corresponds to C-H stretching, 1740 cm^{-1} to C=O stretching, and 1160–1060 cm^{-1} to C-O and C-O-C groups, which is consistent with previously reported data.[22] In the ALN-PLGA-PEG spectrum, the band at 3480 cm^{-1} indicates O-H stretching from ALN, while the band at 3270 cm^{-1} corresponds to N-H stretching of the amide (-CO-NH) bond.[23] Compared with the ALN spectrum, the peaks at 1600 and 1630 cm^{-1} (N-H) were significantly weaker in the ALN-PLGA-PEG spectrum, indicating the substitution of the $-NH_2$ group in ALN and its conjugation with

PLGA-PEG. The band at 1740 cm^{-1} confirmed the presence of the C=O group in the amide structure, and the presence of the C-O group in PLGA-PEG was confirmed by the band at 1060 cm^{-1}.[24] The analysis of ^{1}H NMR spectra was performed on ALN, PLGA-PEG-COOH, and ALN-PLGA-PEG (Supplementary Figure S1A–C). In the ALN-PLGA-PEG spectrum, the peak at 2.26 ppm indicates the methylene protons of ALN,[25] at 1.45 ppm corresponds to the methyl groups of lactic units of PLGA, and 3.58 ppm corresponds to the oxyethylene units of PEG, confirming the successful synthesis of ALN-PLGA-PEG conjugation.[26] The infrared and ^{1}H NMR spectra confirmed the successful synthesis of the ALN-PLGA-PEG conjugates.

TEM images revealed that RPT/PLGA-PEG and RPT/ALN-PLGA-PEG nanosystems appeared spherical, with mean sizes of 85.62 ± 2.14 and 89.38 ± 2.77 nm, respectively, exhibiting a symmetrical distribution (Figure 2C–F). The particle size of the RPT/ALN-PLGA-PEG nanosystems was slightly larger than that of the RPT/PLGA-PEG nanosystems, with no statistically significant difference. Both types of nanoparticles exhibited drug EE exceeding 70%, loading capacity of 6%–7%, PDI ranging from 0.15 to 0.18, and ZP between −15 and −19 mV, indicating good homogeneity (Supplementary Table S1). Stability studies revealed that both nanosystems remained stable for at least 3 months, with no significant differences observed (Supplementary Table S2).

Drug Release Properties in vitro

The release profiles of the RPT/ALN-PLGA-PEG and RPT/PLGA-PEG nanosystems are depicted in Figure 2G and H. An initial burst effect was observed in the release profiles, followed by a sustained and controlled release phase. Conversely, free RPT demonstrated a rapid release pattern, with approximately 80% of the drug released within the first 3 h. At 72 h, the drug concentrations for the RPT/ALN-PLGA-PEG and RPT/PLGA-PEG nanosystems were 4.18 ± 0.19 and 4.76 ± 1.91 μg/mL, respectively, significantly exceeding the minimum inhibitory concentration. Additionally, the cumulative release rates for these nanosystems were 86.69% and 83.95%, respectively. The release kinetics of these nanosystems were analyzed using the zero-order, first-order, and Higuchi equation models. For the RPT/ALN-PLGA-PEG nanosystem, the R-squared values for the zero-order, first-order, and Higuchi equation models were 0.84098, 0.98782, and 0.97155, respectively. For the RPT/PLGA-PEG nanosystems, R-squared values were 0.81489, 0.98815, and 0.95903, respectively. These results imply that the release kinetics of these nanosystems predominantly follow a first-order kinetic model.

In vitro Assessment of Antibacterial Activity and Cytotoxicity

After 3 weeks, the diameters of the antibacterial inhibition zones for free RPT, RPT/PLGA-PEG, and RPT/ALN-PLGA-PEG nanosystems were measured at 18.90 ± 0.20, 18.17 ± 0.31, and 18.53 ± 0.90 mm, respectively, without statistically significant differences. At 4 weeks, the inhibition zone diameters for the RPT/ALN-PLGA-PEG and RPT/PLGA-PEG nanosystems were 18.87 ± 0.55 and 18.50 ± 0.96 mm, respectively (Figure 3A and B), indicating no statistically significant difference between the two formulations. However, the inhibition zone diameter of free RPT was 15.5 ± 0.75 mm, which was significantly lower than those of the nanosystems.

The viability of BMSCs incubated with different concentrations of ALN and RPT for 48 h was assessed using the CCK-8 assay. RPT/ALN-PLGA-PEG and ALN-PLGA-PEG nanosystems maintained cell viability above 90% across all tested ALN concentrations, indicating low cytotoxicity and favorable biocompatibility. Conversely, free ALN at 10 μg/mL resulted in cell viability levels below 85%, indicating that nano-formulation may mitigate the cytotoxicity of ALN (Figure 3C). The cell viability for RPT/ALN-PLGA-PEG and RPT/PLGA-PEG nanosystems exceeded 90% across all tested RPT concentrations, whereas free RPT at 60 μg/mL led to viability below 85%, confirming that nano-formulation may reduce the cytotoxicity of RPT (Figure 3D).

In vitro Cellular Uptake of Nanosystems

Cells treated with RPT/PLGA-PEG and RPT/ALN-PLGA-PEG nanosystems exhibited low fluorescence intensity at 2 h (Figure 3E), with a peak detected at 6 h (Figure 3F). No significant differences were observed in the cellular uptake between the RPT/PLGA-PEG and RPT/ALN-PLGA-PEG nanosystems in BMMs. These results demonstrate that surface

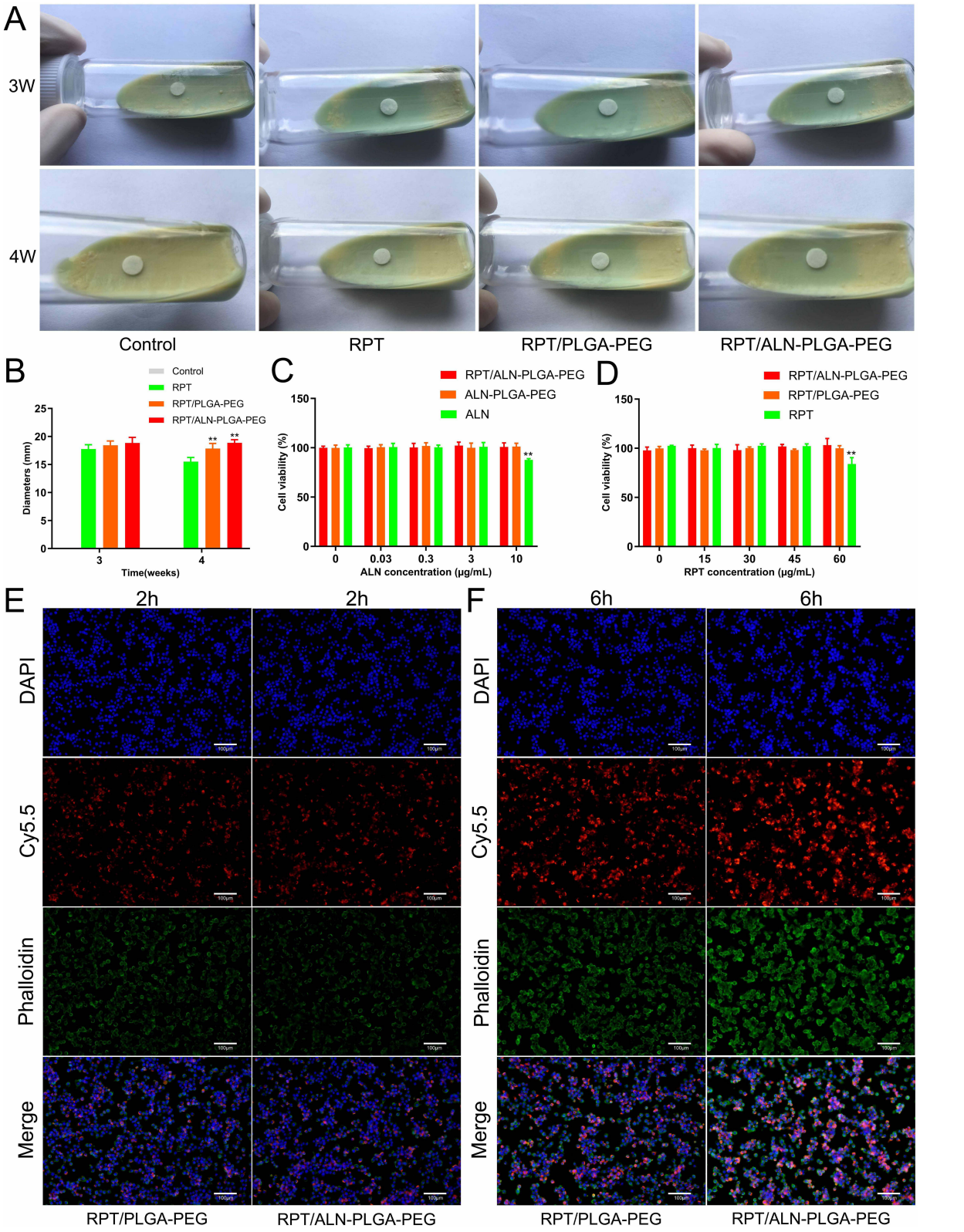

Figure 3 Nanosystems can enhance the antibacterial efficacy of RPT, reduce cytotoxic effects, and promote cellular uptake. Illustration of the antibacterial inhibition zones in the control, RPT, RPT/PLGA-PEG, and RPT/ALN-PLGA-PEG groups (**A**). Quantitative assessment of antibacterial inhibition zone diameters across experimental groups (**B**). **P < 0.01 vs RPT. Cytotoxicity evaluations of ALN-functionalized (**C**) and RPT-loaded (**D**) nanosystems on BMSCs were conducted. **P < 0.01 vs 0 concentration group. Data are presented as mean ± SD (n = 3). The cellular uptake of Cy5-labeled RPT/PLGA-PEG and RPT/ALN-PLGA-PEG nanosystems was assessed using CLSM after incubation periods of 2 hours (**E**) and 6 hours (**F**), respectively (scale bar = 100 μm).

https://doi.org/10.2147/IJN.S478893

modification of nanosystems with ALN molecules confers bone-targeting capability without compromising the cellular uptake efficiency of BMMs.

Evaluation of Nanosystems Biodistribution, Biosafety, and Targeting Efficiency

The drug tissue distribution analysis revealed that RPT concentrations in bone tissue were significantly elevated by at least 3-fold in the RPT/ALN-PLGA-PEG group compared to both the RPT/PLGA-PEG and free RPT groups at 1, 24, and 48 hours post-administration (Figure 4A–C). This finding demonstrates the excellent bone-targeting capability of the RPT/ALN-PLGA-PEG nanosystem. Furthermore, the concentration of RPT delivered by the RPT/ALN-PLGA-PEG nanosystem within bone tissue consistently exceeded that in the bloodstream at all tested time points (Figure 4D). Additionally, at 24 and 48 h post-administration, the concentration of RPT in the bloodstream delivered by the RPT/ALN-PLGA-PEG and RPT/PLGA-PEG nanosystems was significantly higher than that of the free RPT group, indicating that the nanosystems exhibited prolonged release characteristics. Furthermore, serum biomarkers of liver and kidney

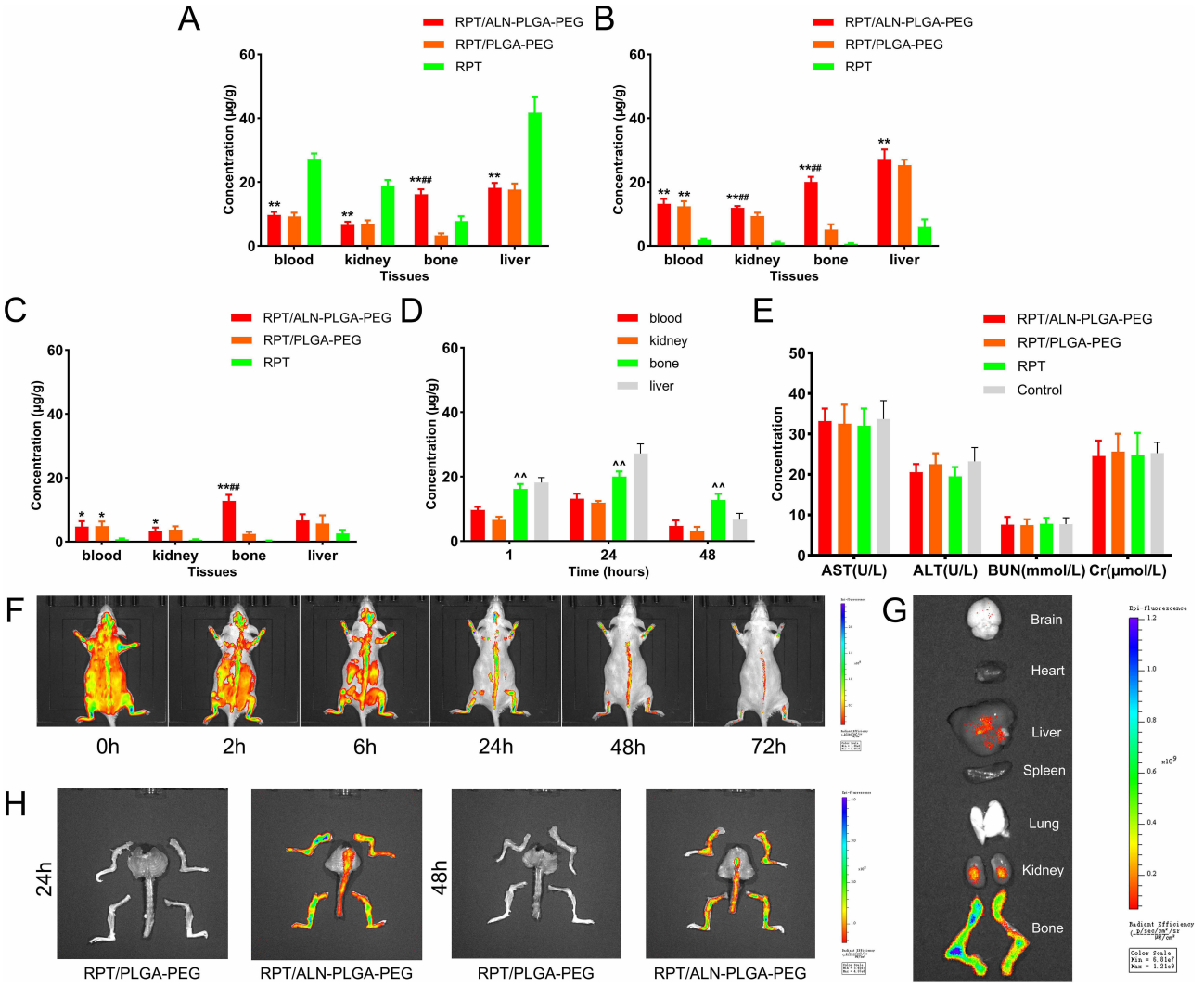

Figure 4 The RPT/ALN-PLGA-PEG nanosystems exhibited a significantly improved accumulation of RPT within bone tissue and demonstrated favorable biocompatibility for in vivo applications. The drug concentration distribution of different formulations across various tissues is illustrated at time intervals of 1 hour (**A**), 24 hours (**B**), and 48 hours (**C**). *P < 0.05, **P < 0.01 vs RPT; ##P < 0.01 vs RPT/PLGA-PEG. The drug concentration of RPT/ALN-PLGA-PEG in various tissues was quantitatively determined at multiple time points (**D**). ^^P < 0.01 vs Blood. Serum biochemical analysis results for AST, ALT, BUN, and Cr following administration of different formulations (**E**). Data are presented as mean ± SD (n=3). In vivo fluorescence imaging of mice was performed at various time points after intravenous administration of RPT/ALN-PLGA-PEG (**F**). Fluorescence imaging of major organs in mice was conducted at 24 hours post-administration of RPT/ALN-PLGA-PEG (**G**). Fluorescence imaging of biodistribution in bone tissue was performed after intravenous administration of RPT/PLGA-PEG and RPT/ALN-PLGA-PEG at 24 hours and 48 hours (**H**).

function, including AST, ALT, BUN, and Cr, were found to be within normal levels (Figure 4E). These toxicological findings suggest that the nanosystems possess an appropriate biosafety profile for in vivo applications. IVIS revealed that RPT/ALN-PLGA-PEG nanosystems were rapidly distributed throughout the mouse body, with significant accumulation in the bone tissue over time (Figure 4F). However, significant hepatic accumulation was observed (Figure 4G). The RPT/ALN-PLGA-PEG nanosystems remained detectable in bone tissue at 24 and 48 h post-injection (Figure 4H). These findings indicate that RPT/ALN-PLGA-PEG nanosystems can efficiently localize to bone tissue following systemic administration and exhibit sustained accumulation within the bone over time.

Evaluation of the Impact of Nanosystems on Cell Differentiation

BMSCs were cultured for 7 d, followed by staining with Alizarin Red and ALP (Figure 5A). All groups demonstrated positive Alizarin Red staining. The other three groups demonstrated a significantly enhanced intensity of Alizarin Red staining than the control group (Figure 5B). A similar trend was observed for ALP staining (Figure 5C). Moreover, BMMs were cultured for 7 days and stained with TRAP (Figure 5A). The analysis revealed a significant reduction in the number of osteoclasts in the other three groups compared to the control group (Figure 5D).

This study investigated the impact of nanosystems on osteogenic and osteoclastic differentiation. Compared to the control group, the levels of collagen I and osteocalcin were significantly elevated in the other three groups (Figure 5E and F). Moreover, the levels of NFATc1 and c-Fos were measured in BMMs using Western blot analysis, revealing that these protein concentrations were significantly decreased in the other three groups compared to those in the control group (Figure 5G and H). The above results demonstrated that the ALN-functionalized nanosystem exhibited dual regulatory capabilities, promoting the osteogenic differentiation of BMSCs while concurrently inhibiting osteoclastogenesis in BMMs.

Evaluation of the Therapeutic Effect of the Nanosystems

During the observation period, CRP levels decreased in all four groups. Notably, the CRP levels in the RPT/ALN-PLGA-PEG group exhibited a significant decrease, with near-normal levels after 2 weeks of treatment (Figure 6A). Conversely, CRP levels in the RPT and RPT/PLGA-PEG groups decreased gradually, approaching normal levels after 8 weeks of treatment. However, the CRP levels in the control group remained significantly higher than normal levels after 8 weeks of treatment. The ESR levels demonstrated consistent trends across all four groups (Figure 6B).

Except for the control group, the mean BMD levels in all other groups increased gradually (Figure 6C). Notably, BMD levels in the RPT/ALN-PLGA-PEG group were not significantly different from the normal levels 1 week after treatment. Contrarily, BMD levels in the other three groups remained below normal throughout the observation period.

Throughout the observation period, the mean serum BALP level gradually increased in all groups except for the control group and the RPT/ALN-PLGA-PEG group (Figure 6D). Notably, BALP levels in the RPT/ALN-PLGA-PEG group were significantly higher than normal levels at 4 weeks post-treatment and subsequently decreased to normal levels by 8 weeks post-treatment. In contrast, the control group demonstrated a gradual increase, reaching normal levels by 8 weeks post-treatment. Similarly, the mean serum P1NP levels exhibited a gradual increase in all groups except for the control group and the RPT/ALN-PLGA-PEG group (Figure 6E). The P1NP levels in the RPT/PLGA-PEG group were significantly higher than the normal levels as early as 2 weeks post-treatment, and then decreased to normal levels by 8 weeks. Furthermore, a consistent downward trend was observed in the bone resorption markers (TRAP-5b and CTX-1) in all groups except the control group (Figure 6F and G). Notably, the levels of these markers normalized within 2 weeks of treatment in the RPT/ALN-PLGA-PEG group. However, the RPT and RPT/PLGA-PEG groups exhibited a gradual decline toward normal levels over an extended observation period.

Histological Evaluation

The assessment of vertebral body destruction and repair was conducted at 4 and 8 weeks of treatment (Figure 7A and B). At 4 weeks, the Control and RPT groups exhibited extensive spinal destruction areas, characterized by severe surrounding bone destruction and the presence of sinuses. Conversely, the RPT/PLGA-PEG group demonstrated a lower degree of bone destruction and sinus formation. The bone affected area in the RPT/ALN-PLGA-PEG group was filled with well-

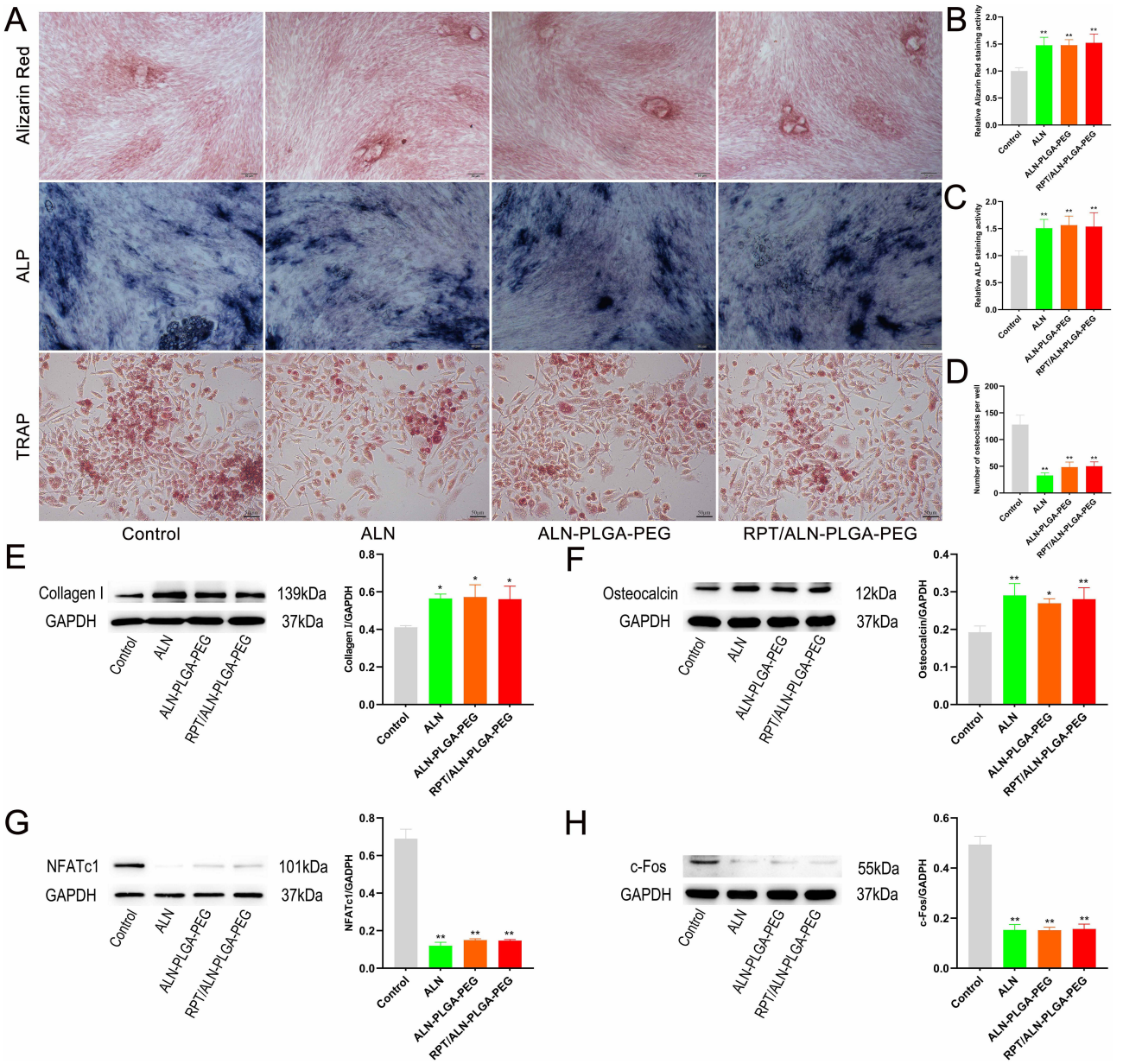

Figure 5 The ALN-functionalized nanosystems demonstrate a dual regulatory capability by promoting the osteogenic differentiation of BMSCs while concurrently inhibiting osteoclastogenesis in BMMs. Representative images of Alizarin Red and ALP staining for BMSCs, and TRAP staining for BMMs (scale bar = 50 μm) (**A**). The Alizarin Red-stained (**B**) and ALP-stained (**C**) areas of cells in each group were quantified using ImageJ software. Statistical analysis of TRAP-positive cell counts in TRAP-stained samples (**D**). **P < 0.01 vs Control. Data are presented as mean ± SD (n = 3). Western blotting analysis revealed that the ALN-functionalized nanosystems significantly enhanced the expression levels of Collagen I (**E**) and Osteocalcin (**F**) in BMSCs. The ALN-functionalized nanosystems significantly inhibited the expression levels of NFATc1 (**G**) and c-Fos (**H**) in BMMs, as demonstrated by Western blotting analysis. *P < 0.05, **P < 0.01 vs Control. Data are presented as mean ± SD (n = 3).

integrated osteoid and bone tissue, indicating a relatively low degree of bone destruction and successful defect repair. By 8 weeks post-treatment, the previously affected areas in the Control, RPT, and RPT/PLGA-PEG groups were predominantly occupied by prominent fibrous-like tissue. Conversely, in the RPT/ALN-PLGA-PEG group, the affected area was entirely replaced by regenerated bone tissue.

The scores recorded for the RPT/ALN-PLGA-PEG group exhibited a statistically significant difference compared to the other three groups at both 4 and 8 weeks post-treatment (Figure 7C). The RPT/ALN-PLGA-PEG group achieved the highest score, whereas the control group exhibited the lowest score throughout the observation period. Additionally, the scores of RPT and RPT/PLGA-PEG groups increased gradually over time.

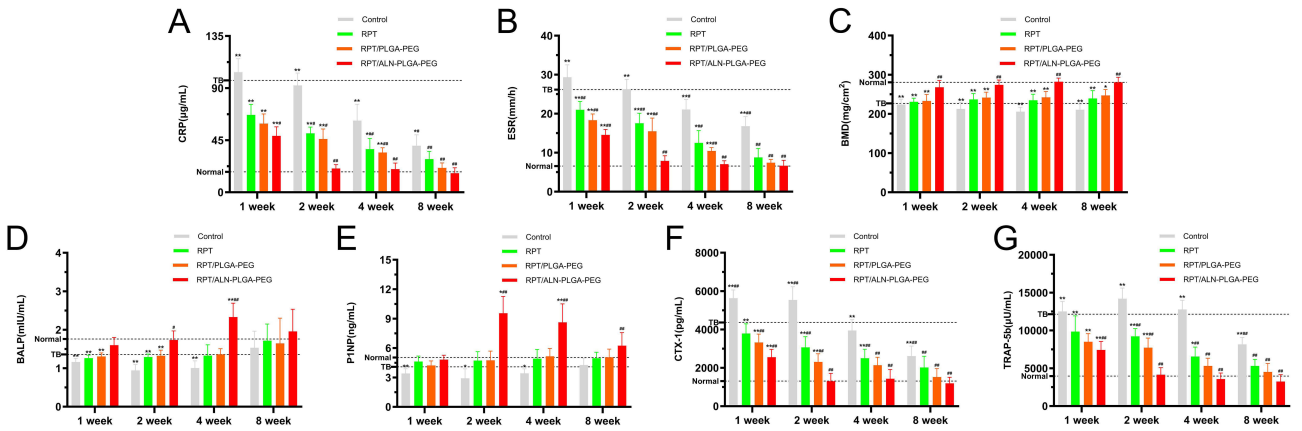

Figure 6 The RPT/ALN-PLGA-PEG nanosystems exhibit a rapid and early ability to alleviate inflammation, promote osteogenesis, inhibit bone resorption, and enhance bone mineral density. In the RPT/ALN-PLGA-PEG group, CRP (**A**) and ESR (**B**) levels significantly decreased and approached normal values within 2 weeks. BMD returned to normal values within 1 week (**C**). BALP levels exceeded normal values at 4 weeks (**D**), while P1NP levels surpassed normal values as early as 2 weeks (**E**). CTX-I (**F**) and TRAP-5b (**G**) levels rapidly declined, reaching near-normal levels within 2 weeks. *P < 0.05, **P < 0.01 vs normal; #P < 0.05, ##P < 0.01 vs TB. Data are presented as mean ± SD (n = 6).

Discussion

Numerous studies have concentrated on the development of diverse nano-delivery systems for anti-TB drugs.[27,28] However, similar research on anti-TB nano-drug delivery systems generally encounters challenges, including low drug delivery efficiency, insufficient concentration in target organs, and unconfirmed therapeutic efficacy.[29] Furthermore, strategies for mitigating bone destruction associated with TB remain to be fully investigated. In this study, ALN was used as a bone-targeting ligand to develop an advanced drug delivery nanosystem (RPT/ALN-PLGA-PEG) specifically designed to target bone tissue. This approach exhibits considerable potential for improving drug safety, prolonging drug release duration, mitigating TB-induced bone destruction and facilitating bone tissue regeneration.

In this study, the ALN-PLGA-PEG conjugate was synthesized using the DCC/NHS technique, resulting in the stable chemical conjugation of ALN to PLGA-PEG. Compared to physical adsorption, chemical coupling is a more effective means of preventing premature detachment of ALN during in vivo circulation.[30] The premix membrane emulsification technique has been extensively used to synthesize nanoparticles with core-shell structures. The significant advantage of this technology is its ability to precisely control the size and morphology of nanoparticles, thereby facilitating the optimization of drug release properties. Compared to previous studies,[31,32] RPT/ALN-PLGA-PEG nanosystems developed using this technology exhibit smaller particle sizes, more uniform particle size distributions, higher EEs, and excellent storage stability.

The zeta potential of the RPT/ALN-PLGA-PEG nanosystem was measured to be −19.03 ± 3.97 mV. A negative zeta potential enhances the in vivo stability by reducing the non-specific adsorption of plasma proteins onto the surface of the nanosystem, thereby minimizing recognition and clearance by the reticuloendothelial system (RES) in both the liver and spleen, which ultimately prolongs systemic circulation time.[33] Furthermore, the negative surface potential can mitigate non-specific adsorption of nanoparticles in vivo, thereby contributing to improved bone-targeting efficiency.[34] Although the drug loading capacity of 6–7% is relatively low compared to some polymer-based nanosystems, the ALN-conjugated bone-targeting specificity allows even minimal doses of nanoparticles to achieve therapeutically effective concentrations in bone tissue. In vivo biodistribution studies indicate that the RPT/ALN-PLGA-PEG formulation attains bone drug concentrations more than 3-fold higher than those observed in the non-targeted group. Furthermore, in vitro release experiments demonstrated sustained drug release over a period of 72 hours, thereby fulfilling the requirements for long-acting treatment. Future research will focus on refining the preparation process, particularly the optimization of the drug-to-carrier ratio, to further enhance loading capacity.

One of the critical factors determining the suitability of nanosystems as drug delivery carriers is their ability to efficiently penetrate target cells.[35] Our results demonstrate that both types of developed nanosystems are efficiently internalized by mononuclear macrophages, which are prevalent at TB infection sites, thereby facilitating passive targeting

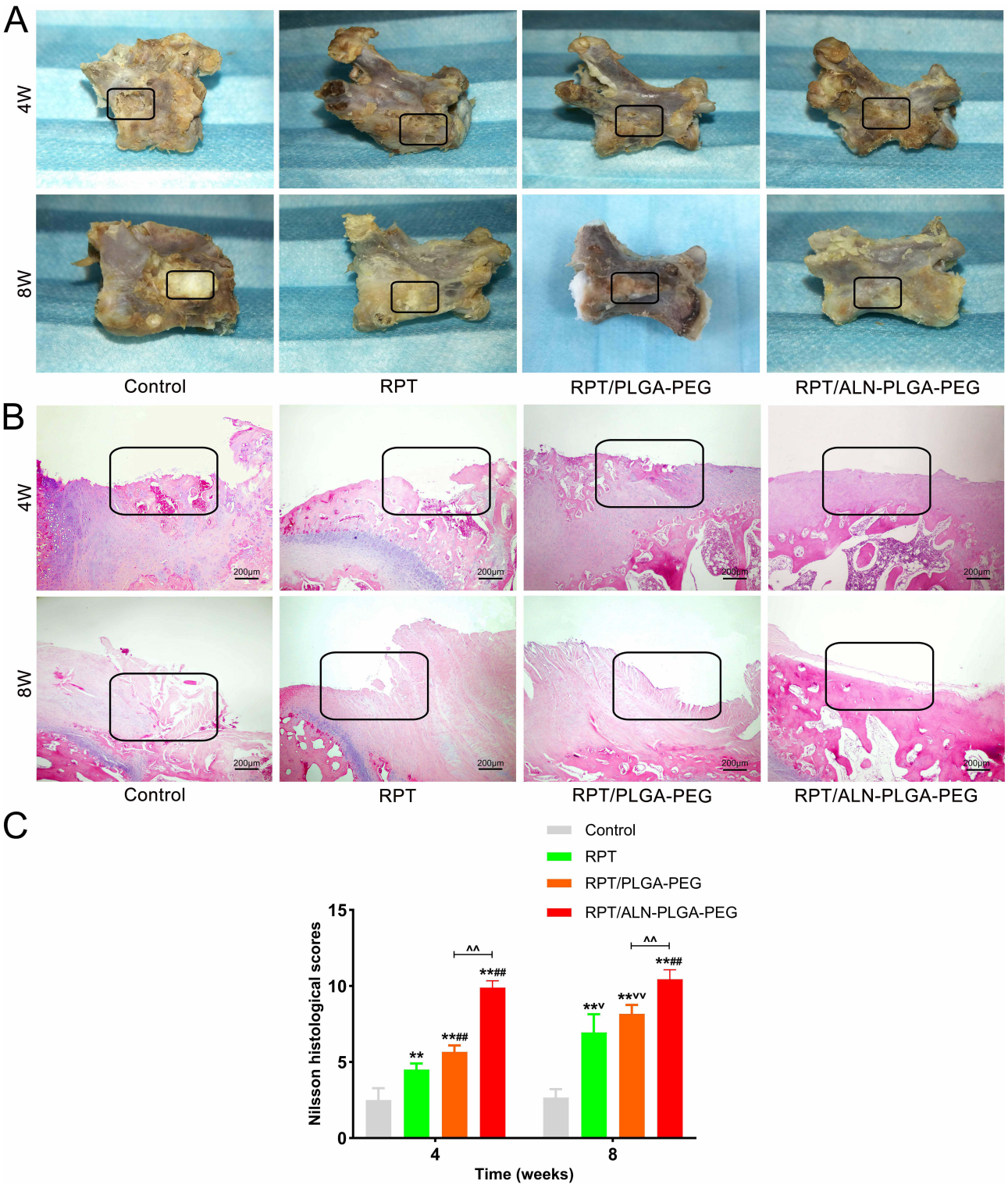

Figure 7 The RPT/ALN-PLGA-PEG nanosystems have demonstrated significant efficacy in the repair of vertebral body destruction. Macroscopic observations indicate that the RPT/ALN-PLGA-PEG group exhibits mild bone destruction, accompanied by effective repair at both 4 and 8 weeks (**A**). Histological examination via HE staining reveals complete replacement of the affected area with regenerated bone tissue in this group at 4 and 8 weeks (scale bar = 200 μm) (**B**). The area delineated by the black box in the image corresponds to the region of spinal destruction. The RPT/ALN-PLGA-PEG group achieved the highest scores compared to other groups at both time points of 4 and 8 weeks (**C**). **P < 0.01 vs Control; $^{\#\#}$P < 0.01 vs RPT; ^^P < 0.01 vs RPT/PLGA-PEG; ^{V}P < 0.05, ^{VV}P < 0.01 vs 4 weeks. Data are presented as mean ± SD (n = 6).

of the drug to lesion tissues. However, the systemic administration of nanosized drugs has led to unexpected side effects.[36,37] A bone-targeting nanosystem could provide a viable solution to this challenge by reducing adverse off-target effects and improving therapeutic efficacy, specifically for bone tissue.[38–41]

The high affinity of the diphosphate structure in ALN for bone minerals significantly improved the bone-targeting efficiency of nanosystems, resulting in a 3–5-fold increase in drug concentration within bone tissue.[42,43] Tissue drug distribution experiments and IVIS revealed that RPT/ALN-PLGA-PEG nanosystems exhibited higher accumulation in bone tissues, indicating that ALN is pivotal for modulating drug distribution. Additionally, nanosystems were detected in various organs, notably the liver and kidneys, which may be due to the blood circulation in these organs facilitating nanoparticle deposition.[35] This study substantiates the dual-targeting properties of the developed drug delivery system, including active and passive targeting mechanisms.

In terms of antibacterial efficacy, this study demonstrated that both RPT-loaded nanosystems exhibited significant advantages over free drug after 4 weeks. These findings imply that nanosystems can effectively suppress *Mycobacterium tuberculosis* infection for an extended duration. Numerous studies have demonstrated that the in vitro antibacterial efficacy of nano-formulations generally surpasses that of free drugs. This phenomenon can be ascribed to the ability of nanostructures with controlled drug release to gradually undermine the resistance of the bacterial membrane over time, thereby increasing bacterial mortality rates.[44] Furthermore, the high specific surface area of nanosystems contributes to their improved capacity to penetrate the cell walls of *Mycobacterium tuberculosis*, representing another key factor that enhances antibacterial performance.[45]

Nanocarriers represent a promising approach for improving drug safety by significantly increasing drug accumulation efficiency at target sites through targeted delivery mechanisms while concurrently minimizing non-specific distribution and associated toxicity.[46,47] A recent study demonstrated that bisphosphonate promotes the osteogenic differentiation of BMSCs in a concentration-dependent manner.[48] However, it inhibits osteoblast proliferation and differentiation at high concentrations due to its cytotoxic effects.[49] This study demonstrated that nanotechnology can effectively reduce the cytotoxicity associated with ALN and RPT. RPT/ALN-PLGA-PEG nanosystems, at a low concentration (3 μg/mL of ALN), promoted the osteogenic differentiation of BMSCs and inhibited osteoclast activity. These findings are consistent with several previous studies and provide critical evidence supporting the application of nanotechnology in the treatment of osteoarticular TB.[50,51]

The rabbit spinal TB model is widely recognized as the most effective for evaluating the efficacy of drugs against osteoarticular TB.[52–54] In this study, this model was used to validate the synergistic effects of RPT and ALN in the RPT/ALN-PLGA-PEG nanosystems for treating spinal TB. ESR and CRP are critical biomarkers for assessing inflammation and stress responses in TB.[55,56] Continuous monitoring of ESR and CRP levels demonstrated that the levels in the RPT/ALN-PLGA-PEG group rapidly normalized, exhibiting a significantly greater improvement compared to the RPT/PLGA-PEG group, which declined gradually. These findings demonstrate that the RPT/ALN-PLGA-PEG nanosystems exhibits improved anti-inflammatory and antibacterial properties. The observed differences may be closely associated with the drug release characteristics of the nanocarriers and the bone-targeting effect of ALN, which significantly enhances drug accumulation at the infection site.[57]

To the best of our knowledge, this is the first study to use serum bone turnover markers (BTMs) to assess bone destruction and remodeling associated with bone TB.[58] BTMs serve as indicators of osteoblastic and osteoclastic activity. Osteoid synthesis by osteoblasts is characterized by BALP and PINP production. The production of CTX-1 degradation fragments and the release of TRACP-5b indicate enzymatic digestion and removal of the bone organic matrix.[59] Our study demonstrated that after 2 weeks of RPT/ALN-PLGA-PEG treatment, CTX-I and TRACP-5b levels normalized, indicating significant inhibition of osteoclast activity and reduction in bone destruction. Simultaneously, PINP levels increased significantly, surpassing the normal range, indicating enhanced osteoblast activity. By the fourth week, the BALP level also increased significantly beyond the normal range, indicating the mineralization phase of bone formation. Interpreting these discrepancies remains challenging; however, alterations in serum BTMs may manifest on different temporal scales than those in osteoblast and osteoclast activity or gene expression.[60] During the first week of treatment with RPT/ALN-PLGA-PEG, the BMD level was significantly elevated compared to the other groups and approached normal levels. This observation demonstrates that bone destruction associated with bone TB was effectively mitigated.

Previous studies have demonstrated that ALN prevents bone destruction by modulating osteoclast formation and function, as well as inhibiting bone resorption.[61]

Histological observations and NHS results demonstrated that bone destruction was repaired more effectively in the RPT/ALN-PLGA-PEG group than in the other three groups. This advantage can be ascribed to its unique dual mechanism of action. First, ALN, a bone-targeting drug ligand, significantly increases the local drug concentration within bone tissue.[62] Nevertheless, non-targeted drugs cannot penetrate the bone tissue, resulting in suboptimal local drug concentrations at the lesion site. This deficiency leads to abnormal secretion of growth factors, chemokines, and inflammatory factors, which adversely affect the migratory activity and osteogenic differentiation potential of BMSCs.[63,64] Moreover, the persistent presence of inflammatory cells directly suppresses the ALP activity of BMSCs and mineralization-related gene expression through the secretion of inflammatory factors.[65] This inhibition hinders bone matrix synthesis, ultimately leading to the replacement of the bone defect area with fibrous connective tissue rather than complete bone regeneration. Second, analysis of serum BTMs and BMD assessment demonstrated that ALN in this formulation specifically inhibited osteoclast activity, significantly reduced bone destruction associated with bone TB, and facilitated the systematic repair of bone tissue by providing favorable conditions.

However, this study has several limitations. First, the rabbit model of spinal tuberculosis exhibited inconsistent lesion severity, which may have contributed to inter-individual variability in therapeutic responses. Second, the molecular mechanisms underlying the RPT/ALN-PLGA-PEG nanosystem's promotion of bone tissue regeneration remain incompletely elucidated. In particular, the regulatory roles of inflammation-related signaling pathways, such as nuclear factor kappa B (NF-κB) and RANKL, in maintaining the dynamic balance between bone resorption and bone formation warrant further investigation. Furthermore, the long-term efficacy and safety profile of this therapeutic strategy require validation through more comprehensive and systematic studies.

Conclusion

In conclusion, the bone-targeted nanosystems developed in this study via the premix membrane emulsification technique exhibited excellent quality, characterized by small and uniformly distributed particle sizes, smooth surface morphology, and excellent storage stability. This nanosystem demonstrates significant multifaceted advantages in the treatment of osteoarticular TB, including precise drug delivery facilitated by the bone-targeting properties of ALN, sustained and potent antibacterial efficacy attributed to the characteristics of the nanosystem, and mitigation of bone destruction coupled with promotion of bone repair through inhibition of osteoclast activity. Furthermore, this study validated the synergistic effects of RPT and ALN in the RPT/ALN-PLGA-PEG nanosystems for treating osteoarticular TB. These findings indicate that the RPT/ALN-PLGA-PEG bone-targeted nanosystems is a promising therapeutic strategy with significant potential for clinical application in treating osteoarticular TB and promoting bone health.

Acknowledgments

We thank Home for Researchers editorial team (www.home-for-researchers.com) for language editing service.

Funding

This study is supported by the Four "Batches" Innovation Project of Invigorating Medical through Science and Technology of Shanxi Province (Grant No. 2022XM50); Shanxi Province Science Foundation for Youths (Grant No. 202303021212516); Health and Hygiene Research Projects of Shanxi Province (Grant No. 2022076).

Disclosure

The authors report no conflicts of interest in this work.

References

1. Jain AK, Rajasekaran S, Jaggi KR, Myneedu VP. Tuberculosis of the spine. *J Bone Joint Surg Am*. 2020;102(7):617–628. doi:10.2106/JBJS.19.00001
2. Snow KJ, Cruz AT, Seddon JA, et al. Adolescent tuberculosis. *Lancet Child Adolesc Health*. 2020;4(1):68–79. doi:10.1016/S2352-4642(19)30337-2

3. Ukunda UNF, Lukhele MM. The posterior-only surgical approach in the treatment of tuberculosis of the spine: outcomes using cortical bone allografts. *Bone Joint J*. 2018;100-b(9):1208–1213. doi:10.1302/0301-620X.100B9.BJJ-2017-1326.R2
4. Sukhithasri V, Vinod V, Varma S, Biswas R. Mycobacterium tuberculosis treatment modalities and recent insights. *Curr Drug Deliv*. 2014;11(6):744–752. doi:10.2174/1567201811666140619121728
5. Patra JK, Das G, Fraceto LF, et al. Nano based drug delivery systems: recent developments and future prospects. *J Nanobiotechnology*. 2018;16(1):71. doi:10.1186/s12951-018-0392-8
6. Kim KT, Lee JY, Kim DD, Yoon IS, Cho HJ. Recent progress in the development of poly(lactic-co-glycolic acid)-based nanostructures for cancer imaging and therapy. *Pharmaceutics*. 2019;11(6):280. doi:10.3390/pharmaceutics11060280
7. Luque-Michel E, Imbuluzqueta E, Sebastián V, Blanco-Prieto MJ. Clinical advances of nanocarrier-based cancer therapy and diagnostics. *Expert Opin Drug Deliv*. 2017;14(1):75–92. doi:10.1080/17425247.2016.1205585
8. Pala R, Barui AK, Mohieldin AM, Zhou J, Nauli SM. Folate conjugated nanomedicines for selective inhibition of mTOR signaling in polycystic kidneys at clinically relevant doses. *Biomaterials*. 2023;302:122329. doi:10.1016/j.biomaterials.2023.122329
9. Alfarisi O, Alghamdi WA, Al-Shaer MH, Dooley KE, Peloquin CA. Rifampin vs. rifapentine: what is the preferred rifamycin for tuberculosis? *Expert Rev Clin Pharmacol*. 2017;10(10):1027–1036. doi:10.1080/17512433.2017.1366311
10. Meghji S, White PA, Nair SP, et al. Mycobacterium tuberculosis chaperonin 10 stimulates bone resorption: a potential contributory factor in Pott's disease. *J Exp Med*. 1997;186(8):1241–1246. doi:10.1084/jem.186.8.1241
11. Liu W, Zhou J, Niu F, et al. Mycobacterium tuberculosis infection increases the number of osteoclasts and inhibits osteoclast apoptosis by regulating TNF-α-mediated osteoclast autophagy. *Exp Ther Med*. 2020;20(3):1889–1898. doi:10.3892/etm.2020.8903
12. Panahifar A, Mahmoudi M, Doschak MR. Synthesis and in vitro evaluation of bone-seeking superparamagnetic iron oxide nanoparticles as contrast agents for imaging bone metabolic activity. *ACS Appl Mater Interfaces*. 2013;5(11):5219–5226. doi:10.1021/am4010495
13. Thomopoulos S, Matsuzaki H, Zaegel M, Gelberman RH, Silva MJ. Alendronate prevents bone loss and improves tendon-to-bone repair strength in a canine model. *J Orthop Res*. 2007;25(4):473–479. doi:10.1002/jor.20293
14. Cattalini JP, Boccaccini AR, Lucangioli S, Mouriño V. Bisphosphonate-based strategies for bone tissue engineering and orthopedic implants. *Tissue Eng Part B Rev*. 2012;18(5):323–340. doi:10.1089/ten.teb.2011.0737
15. Wang Z, Maimaitiaili A, Wang T, Song X. Rifapentine polylactic acid sustained-release microsphere complex for spinal tuberculosis therapy: preparation, in vitro and in vivo studies. *Infect Drug Resist*. 2021;14:1781–1794. doi:10.2147/IDR.S304864
16. Kim HK, Kim JH, Abbas AA, Yoon TR. Alendronate enhances osteogenic differentiation of bone marrow stromal cells: a preliminary study. *Clin Orthop Relat Res*. 2009;467(12):3121–3128. doi:10.1007/s11999-008-0409-y
17. Kuljanin J, Janković I, Nedeljković J, Prstojević D, Marinković V. Spectrophotometric determination of alendronate in pharmaceutical formulations via complex formation with Fe(III) ions. *J Pharm Biomed Anal*. 2002;28(6):1215–1220. doi:10.1016/S0731-7085(02)00021-3
18. Rifat D, Prideaux B, Savic RM, et al. Pharmacokinetics of rifapentine and rifampin in a rabbit model of tuberculosis and correlation with clinical trial data. *Sci Transl Med*. 2018;10(435). doi:10.1126/scitranslmed.aai7786
19. Wang Z, Song X, Yang H, Maimaitiaili A, Wang T. Development and in vitro characterization of rifapentine microsphere-loaded bone implants: a sustained drug delivery system. *Ann Palliat Med*. 2020;9(2):375–387. doi:10.21037/apm.2020.03.13
20. Nilsson OS, Urist MR, Dawson EG, Schmalzried TP, Finerman GA. Bone repair induced by bone morphogenetic protein in ulnar defects in dogs. *J Bone Joint Surg Br*. 1986;68(4):635–642. doi:10.1302/0301-620X.68B4.3733844
21. Liu X, Qu S, Lu X, Ge X, Leng Y. Time-of-flight secondary ion mass spectrometry study on the distribution of alendronate sodium in drug-loaded ultra-high molecular weight polyethylene. *Biomed Mater*. 2009;4(6):065008. doi:10.1088/1748-6041/4/6/065008
22. Ge Z, Ma R, Xu G, et al. Development and in vitro release of isoniazid and rifampicin-loaded bovine serum albumin nanoparticles. *Med Sci Monit*. 2018;24:473–478. doi:10.12659/MSM.905581
23. Hwang S-J, Lee J-S, Ryu T-K, et al. Alendronate-modified hydroxyapatite nanoparticles for bone-specific dual delivery of drug and bone mineral. *Macromol Res*. 2016;24(7):623–628. doi:10.1007/s13233-016-4094-5
24. Thakur CK, Thotakura N, Kumar R, et al. Chitosan-modified PLGA polymeric nanocarriers with better delivery potential for tamoxifen. *Int J Biol Macromol*. 2016;93(Pt A):381–389. doi:10.1016/j.ijbiomac.2016.08.080
25. Jing C, Li B, Tan H, et al. Alendronate-decorated nanoparticles as bone-targeted alendronate carriers for potential osteoporosis treatment. *ACS Appl Bio Mater*. 2021;4(6):4907–4916. doi:10.1021/acsabm.1c00199
26. Xie Y, Liu C, Huang H, et al. Bone-targeted delivery of simvastatin-loaded PEG-PLGA micelles conjugated with tetracycline for osteoporosis treatment. *Drug Deliv Transl Res*. 2018;8(5):1090–1102. doi:10.1007/s13346-018-0561-1
27. Prabhu P, Fernandes T, Chaubey P, et al. Mannose-conjugated chitosan nanoparticles for delivery of Rifampicin to Osteoarticular tuberculosis. *Drug Deliv Transl Res*. 2021;11(4):1509–1519. doi:10.1007/s13346-021-01003-7
28. Liu P, Guo B, Wang S, Ding J, Zhou W. A thermo-responsive and self-healing liposome-in-hydrogel system as an antitubercular drug carrier for localized bone tuberculosis therapy. *Int J Pharm*. 2019;558:101–109. doi:10.1016/j.ijpharm.2018.12.083
29. Liang Q, Zhang P, Zhang L, et al. Development of tetracycline-modified nanoparticles for bone-targeted delivery of anti-tubercular drug. *Front Bioeng Biotechnol*. 2023;11:1207520. doi:10.3389/fbioe.2023.1207520
30. Feng S, Wu ZX, Zhao Z, et al. Engineering of bone- and CD44-dual-targeting redox-sensitive liposomes for the treatment of orthotopic osteosarcoma. *ACS Appl Mater Interfaces*. 2019;11(7):7357–7368. doi:10.1021/acsami.8b18820
31. Haque S, Boyd BJ, McIntosh MP, Pouton CW, Kaminskas LM, Whittaker M. Suggested procedures for the reproducible synthesis of poly(d, l-lactide-co-glycolide) nanoparticles using the emulsification solvent diffusion platform. *Curr Nanosci*. 2018;14(5):448–453. doi:10.2174/1573413714666180313130235
32. Dalvi BR, Siddiqui EA, Syed AS, et al. Nevirapine loaded core shell gold nanoparticles by double emulsion solvent evaporation: in vitro and in vivo evaluation. *Curr Drug Deliv*. 2016;13(7):1071–1083. doi:10.2174/1567201813666160114093005
33. Yang A, Yang L, Liu W, Li Z, Xu H, Yang X. Tumor necrosis factor alpha blocking peptide loaded PEG-PLGA nanoparticles: preparation and in vitro evaluation. *Int J Pharm*. 2007;331(1):123–132. doi:10.1016/j.ijpharm.2006.09.015
34. Dinakaran D, Sengupta J, Pink D, et al. PEG-PLGA nanospheres loaded with nanoscintillators and photosensitizers for radiation-activated photodynamic therapy. *Acta Biomater*. 2020;117:335–348. doi:10.1016/j.actbio.2020.09.029

35. Gao W, Li JJ, Shi J, Lan H, Guo Y, Fu D. Ångstrom-scale gold particles loaded with alendronate via alpha-lipoic acid alleviate bone loss in osteoporotic mice. *J Nanobiotechnology*. 2024;22(1):212. doi:10.1186/s12951-024-02466-9
36. Li K, Zhuang P, Tao B, Li D, Xing X, Mei X. Ultra-small lysozyme-protected gold nanoclusters as nanomedicines inducing osteogenic differentiation. *Int J Nanomed*. 2020;15:4705–4716. doi:10.2147/IJN.S241163
37. Bolaños K, Kogan MJ, Araya E. Capping gold nanoparticles with albumin to improve their biomedical properties. *Int J Nanomed*. 2019;14:6387–6406. doi:10.2147/IJN.S210992
38. Rosenblum D, Joshi N, Tao W, Karp JM, Peer D. Progress and challenges towards targeted delivery of cancer therapeutics. *Nat Commun*. 2018;9(1):1410. doi:10.1038/s41467-018-03705-y
39. Järvinen TA, Ruoslahti E. Target-seeking antifibrotic compound enhances wound healing and suppresses scar formation in mice. *Proc Natl Acad Sci U S A*. 2010;107(50):21671–21676. doi:10.1073/pnas.1016233107
40. Hu CM, Fang RH, Wang KC, et al. Nanoparticle biointerfacing by platelet membrane cloaking. *Nature*. 2015;526(7571):118–121. doi:10.1038/nature15373
41. Vanderburgh J, Hill JL, Gupta MK, et al. Tuning ligand density to optimize pharmacokinetics of targeted nanoparticles for dual protection against tumor-induced bone destruction. *ACS Nano*. 2020;14(1):311–327. doi:10.1021/acsnano.9b04571
42. Li Z, Xiao X, Pu X, et al. Bone-targeting nucleic acid delivery polymer vector for effective therapy of bone metastasis. *ACS Nano*. 2025;19(17):17014–17027. doi:10.1021/acsnano.5c04743
43. Salerno M, Cenni E, Fotia C, et al. Bone-targeted doxorubicin-loaded nanoparticles as a tool for the treatment of skeletal metastases. *Curr Cancer Drug Targets*. 2010;10(7):649–659. doi:10.2174/156800910793605767
44. Ebrahimi S, Farhadian N, Karimi M, Ebrahimi M. Enhanced bactericidal effect of ceftriaxone drug encapsulated in nanostructured lipid carrier against gram-negative Escherichia coli bacteria: drug formulation, optimization, and cell culture study. *Antimicrob Resist Infect Control*. 2020;9(1):28. doi:10.1186/s13756-020-0690-4
45. Liang Q, Xiang H, Li X, et al. Development of rifapentine-loaded PLGA-based nanoparticles: in vitro characterisation and in vivo study in mice. *Int J Nanomed*. 2020;15:7491–7507. doi:10.2147/IJN.S257758
46. Lim SB, Banerjee A, Önyüksel H. Improvement of drug safety by the use of lipid-based nanocarriers. *J Control Release*. 2012;163(1):34–45. doi:10.1016/j.jconrel.2012.06.002
47. Zheng RR, Zhao LP, Liu LS, et al. Self-delivery nanomedicine to overcome drug resistance for synergistic chemotherapy. *Biomater Sci*. 2021;9(9):3445–3452. doi:10.1039/D1BM00119A
48. Casado-Díaz A, Santiago-Mora R, Dorado G, Quesada-Gómez JM. Risedronate positively affects osteogenic differentiation of human mesenchymal stromal cells. *Arch Med Res*. 2013;44(5):325–334. doi:10.1016/j.arcmed.2013.05.002
49. Huang KC, Cheng CC, Chuang PY, Yang TY. The effects of zoledronate on the survival and function of human osteoblast-like cells. *BMC Musculoskelet Disord*. 2015;16:355. doi:10.1186/s12891-015-0818-5
50. Martins CA, Leyhausen G, Volk J, Geurtsen W. Effects of alendronate on osteoclast formation and activity in vitro. *J Endod*. 2015;41(1):45–49. doi:10.1016/j.joen.2014.07.010
51. Eslami B, Zhou S, Van Eekeren I, LeBoff MS, Glowacki J. Reduced osteoclastogenesis and RANKL expression in marrow from women taking alendronate. *Calcif Tissue Int*. 2011;88(4):272–280. doi:10.1007/s00223-011-9473-5
52. Qiao YJ, Song XY, Zhang LD, Li F, Zhang HQ, Zhou SH. Comparative study of a rabbit model of spinal tuberculosis using different concentrations of Mycobacterium tuberculosis. *World J Orthop*. 2025;16(1):101424. doi:10.5312/wjo.v16.i1.101424
53. Jia J, Zhang M, Cao Z, et al. The rabbit model for spinal tuberculosis: An overview. *J Orthop Surg*. 2024;32(2):10225536241266703. doi:10.1177/10225536241266703
54. Liu X, Wang Y, Jia W. Early diagnosis of spinal tuberculosis by magnetic resonance: perfusion weighted imaging in a rabbit model. *BMC Med Imaging*. 2022;22(1):142. doi:10.1186/s12880-022-00870-x
55. Ding RD, Zhang HJ. Effect of linezolid on serum PCT, ESR, and CRP in patients with pulmonary tuberculosis and pneumonia. *Medicine*. 2018;97(37):e12177. doi:10.1097/MD.0000000000012177
56. Abakay O, Abakay A, Sen HS, Tanrikulu AC. The relationship between inflammatory marker levels and pulmonary tuberculosis severity. *Inflammation*. 2015;38(2):691–696. doi:10.1007/s10753-014-9978-y
57. Lueth P, Haughney SL, Binnebose AM, et al. Nanotherapeutic provides dose sparing and improved antimicrobial activity against Brucella melitensis infections. *J Control Release*. 2019;294:288–297. doi:10.1016/j.jconrel.2018.12.024
58. Schini M, Vilaca T, Gossiel F, Salam S, Eastell R. Bone turnover markers: basic biology to clinical applications. *Endocr Rev*. 2023;44(3):417–473. doi:10.1210/endrev/bnac031
59. Eastell R, Szulc P. Use of bone turnover markers in postmenopausal osteoporosis. *Lancet Diabetes Endocrinol*. 2017;5(11):908–923. doi:10.1016/S2213-8587(17)30184-5
60. Osipov B, Emami AJ, Cunningham HC, et al. Altered post-fracture systemic bone loss in a mouse model of osteocyte dysfunction. *JBMR Plus*. 2024;8(12):ziae135. doi:10.1093/jbmrpl/ziae135
61. Shaalan AAM, El-Sherbiny M, El-Abaseri TB, et al. Supplement with calcium or alendronate suppresses osteopenia due to long term rabeprazole treatment in female mice: influence on bone TRAP and osteopontin levels. *Front Pharmacol*. 2020;11:583. doi:10.3389/fphar.2020.00583
62. Cole LE, Vargo-Gogola T, Roeder RK. Targeted delivery to bone and mineral deposits using bisphosphonate ligands. *Adv Drug Deliv Rev*. 2016;99(Pt A):12–27. doi:10.1016/j.addr.2015.10.005
63. Su P, Tian Y, Yang C, et al. Mesenchymal stem cell migration during bone formation and bone diseases therapy. *Int J Mol Sci*. 2018;19(8):2343. doi:10.3390/ijms19082343
64. Safari B, Davaran S, Aghanejad A. Osteogenic potential of the growth factors and bioactive molecules in bone regeneration. *Int J Biol Macromol*. 2021;175:544–557. doi:10.1016/j.ijbiomac.2021.02.052
65. Lacey DC, Simmons PJ, Graves SE, Hamilton JA. Proinflammatory cytokines inhibit osteogenic differentiation from stem cells: implications for bone repair during inflammation. *Osteoarthritis Cartilage*. 2009;17(6):735–742. doi:10.1016/j.joca.2008.11.011

International Journal of Nanomedicine

Dovepress
Taylor & Francis Group

Publish your work in this journal

The International Journal of Nanomedicine is an international, peer-reviewed journal focusing on the application of nanotechnology in diagnostics, therapeutics, and drug delivery systems throughout the biomedical field. This journal is indexed on PubMed Central, MedLine, CAS, SciSearch®, Current Contents®/Clinical Medicine, Journal Citation Reports/Science Edition, EMBase, Scopus and the Elsevier Bibliographic databases. The manuscript management system is completely online and includes a very quick and fair peer-review system, which is all easy to use. Visit http://www.dovepress.com/testimonials.php to read real quotes from published authors.

Submit your manuscript here: https://www.dovepress.com/international-journal-of-nanomedicine-journal